Journal of
Manufacturing and Materials Processing

MDPI

Article

Enhancement of Additively Manufactured Bagasse Fiber-Reinforced Composite Material Properties Utilizing a Novel Fiber Extraction Process Used for 3D SLA Printing

Md. Shahnewaz Bhuiyan [1,*], Ahmed Fardin [2], M. Azizur Rahman [3], Arafath Mohiv [1], Rashedul Islam [1], Md. Kharshiduzzaman [1], Md. Ershad Khan [4] and Mohammad Rejaul Haque [1]

[1] Department of Mechanical and Production Engineering, Ahsanullah University of Science and Technology, Dhaka 1208, Bangladesh; arafathmohivmunna@gmail.com (A.M.); rashedszahsan7090@gmail.com (R.I.); kharshid.mpe@aust.edu (M.K.); md.rejaulh37.mpe@aust.edu (M.R.H.)
[2] Center for Business, George Brown College, Toronto, ON M5A 3W8, Canada; ahmed.fardin@georgebrown.ca
[3] BRAC Business School, BRAC University, Dhaka 1212, Bangladesh; azizur.rahman@bracu.ac.bd
[4] Department of Textile Engineering, Ahsanullah University of Science and Technology, Dhaka 1208, Bangladesh; ershad.dtt@aust.edu
* Correspondence: newaz.mpe@aust.edu; Tel.: +880-1795571619

Abstract: The growing interest in sustainable and biodegradable materials has prompted significant attention towards natural fiber-reinforced composites (FRC) due to their lower environmental impacts. In a similar sustainable vein, this study fabricated composite materials utilizing bagasse fibers with the 3D SLA (Stereolithography) printing method. To start with, a novel fiber extraction process was adopted for extracting fiber from the bagasse stem in three distinct methods (Process-1, Process-2, and Process-3). The fiber extraction process includes washing, sun-drying, manual collection of rind fibers, immersion of rind fibers in NaOH at specific concentrations for specific durations, combing, and drying. In Process-1, the rind fibers were immersed in 5% NaOH for 15 h, while in Process-2 and Process-3, the rind fibers were immersed in 1% NaOH, but the soaking time varied: 25 h for Process-2 and 18 h for Process-3.for 25 h, and in Process-3, the rind fibers were immersed in 1% NaOH for 18 h. The resulting bagasse fibers underwent comprehensive property assessment with a focus on functional group analysis, diameter measurement, and tensile strength assessment. Subsequently, these fibers were used to fabricate composite materials via the 3D SLA printing technique after being treated in a NaOH solution. The Fourier Transform Infrared (FTIR) Spectroscopy results clearly showed that a fraction of hemicellulose and lignin was removed by NaOH, resulting in improved tensile strength of the bagasse fibers. Three-dimensional-printed composites reinforced with bagasse fibers extracted through the P1 method showed the highest improvement in tensile strength (approximately 70%) compared to specimens made from pure resin. The lack of pores in the composite and the observable fiber fracture phenomena clearly indicate that 3D printing technology effectively enhances the quality of the interface between the fiber and the matrix interfacial bonding, consequently resulting in improved tensile properties of the composites. The 3D-printed composites reinforced with bagasse fiber showcased impressive tensile properties and provided solutions to the limitations of traditional composite manufacturing methods. This sets the stage for developing innovative composite materials that combine natural fibers with cutting-edge fabrication techniques, offering a promising path to tackle present and future economic and ecological challenges.

Keywords: additive manufacturing; bagasse fiber; tensile properties; FTIR analysis; fiber fracture; interfacial adhesion

check for updates

Citation: Bhuiyan, M.S.; Fardin, A.; Rahman, M.A.; Mohiv, A.; Islam, R.; Kharshiduzzaman, M.; Khan, M.E.; Haque, M.R. Enhancement of Additively Manufactured Bagasse Fiber-Reinforced Composite Material Properties Utilizing a Novel Fiber Extraction Process Used for 3D SLA Printing. *J. Manuf. Mater. Process.* **2024**, *8*, 185. https://doi.org/10.3390/jmmp8050185

Academic Editor: Guido Di Bella

Received: 6 July 2024
Revised: 14 August 2024
Accepted: 21 August 2024
Published: 23 August 2024

Copyright: © 2024 by the authors. Licensee MDPI, Basel, Switzerland. This article is an open access article distributed under the terms and conditions of the Creative Commons Attribution (CC BY) license (https://creativecommons.org/licenses/by/4.0/).

1. Introduction

Fiber-reinforced composite materials are created by combining a polymer matrix with high-strength fibers, which may be synthetic, natural, or a blend of both [1]. This

development represents a paradigm shift in materials science, providing a combination of lightweight, a high-strength-to-weight ratio, corrosion resistance, and design flexibility properties to materials that have revolutionized numerous industries [2]. In the last twenty years, significant research has been dedicated to synthetic fiber-reinforced polymer composite materials, including glass, carbon, Kevlar, and basalt fibers. These efforts have been particularly aimed at developing composites with outstanding strength and stiffness [3], making them highly suitable for applications in the aerospace and automotive industries [4]. Despite their beneficial attributes, the fibers used in these composites are expensive, energy-intensive, and non-recyclable [5]. Increased awareness of environmental issues, particularly the escalating greenhouse effect, has spurred significant interest in natural fiber-reinforced composite materials as alternatives to their conventional synthetic counterparts [6]. Natural fibers, originating from renewable plant sources, provide numerous benefits over synthetic fibers. These include biodegradability, renewability, reduced toxicity, a lower carbon footprint in production, lightweight, and the opportunity to upcycle agricultural waste as raw material, in addition to supporting local agriculture [7]. Additionally, if used to replace heavy metallic vehicle components, these lightweight natural materials would curb fuel consumption, further reducing CO_2 emissions [8]. Owing to these benefits, a recent surge in research interest has been noticed in the exploration of natural fibers as potential reinforcing materials for composite development [9,10]. Some of the commonly used natural fibers in composite production include flax, abaca, hemp, sisal, jute, pineapple leaves, oil palm, rice husks, coir, bamboo, and bagasse [5]. Among these, bagasse (the byproduct of sugarcane processing) appears to be a promising material because it is inexpensive, available abundantly, and possesses a significant potential as a perennial crop [11].

In Bangladesh, sugarcane juice is a refreshing beverage, especially during hot and humid summers, extracted by pressing sugarcane stalks. The crop is also used in the production of raw sugar and jaggery. However, following the extraction of the juice, the fibrous residue known as "bagasse" is often improperly disposed of or downcycled, leading to pollution and a loss of economic value. Inadequate waste management practices mostly include the burning of bagasse as fuel or landfill dumping. One superior strategy involves upcycling these fibers for value-added applications, such as reinforcing polymer composites [10].

Bagasse fibers, like other plant-based natural fibers, are primarily composed of 50% cellulose, 25% hemicellulose, and 25% lignin with trace amounts of pectin, waxes, oils, and other extractives [12]. Cellulose provides the fibers with strength, rigidity, and resilience, making them suitable for applications requiring mechanical robustness [12]. On the other hand, hemicellulose enhances the flexibility of the fibers, improving their ability to form composite materials and absorb water [12]. Lignin acts as a binding agent, bringing together cellulose and hemicellulose in the plant cell walls, thus acting as a natural adhesive that enhances cohesion and resistance to external forces. Owing to these befitting characteristics, a substantial amount of research interest in recent years has been directed toward the utilization of bagasse fibers as reinforcement for composite development [11]. Past research on bagasse-reinforced composite materials can be categorized into two main areas: (i) improving interfacial bonding between the fiber and the matrix and (ii) enhancing manufacturing processes to minimize porosity and enhance mechanical strength. Interfacial bonding between the fiber and the matrix has been shown to be enhanced via chemical treatments such as alkali, potassium permanganate, acetylation, silane treatment, benzoylation, acetone treatment, and acrylation [13–16]. Such fiber treatment, along with fiber extraction methods, is also crucial for the enhancement of the mechanical properties of the composite [14,15,17].

On the other hand, manufacturing defects, particularly voids, which are common during the processing of fiber-reinforced composites, can influence the mechanical performance of the composite under service load [18]. Therefore, to minimize these voids in bagasse-reinforced composite materials, various conventional composite manufacturing techniques, including hand layup, compression molding, extrusion, injection molding, and resin transfer molding have been employed. Studies indicate that hand layup with vacuum bagging processes typically yield about 7% voids, while hand layup with cold curing results in approximately 12% voids. Hand layup combined with compression molding can produce around 30% voids, while vacuum bagging alone typically yields about 14% voids. Injection molding typically results in approximately 3% voids, while resin transfer molding processes typically contain about 2% voids [18], indicating that void formation depends on the manufacturing technique used.

Non-conventional techniques like additive manufacturing (also known as 3D printing), particularly Fused Deposition Modeling (FDM) and Stereolithography (SLA), have also been explored in the fabrication of biocomposites [19]. In FDM, a biocomposite filament is deposited layer by layer to build a 3D object. Alternatively, SLA utilizes an ultraviolet projector to harden a photosensitive resin layer by layer, forming the desired object [20]. Though FDM stands out as the most popular and widely utilized additive manufacturing method [21], the literature review indicates several challenges associated with FDM-based printing. Firstly, since FDM operates around 300 °C, selecting a thermoplastic material with a melting temperature below 200 °C to prevent degradation of natural fibers can be challenging [22,23]. Additional hurdles include achieving homogeneous mixing of filler and polymer matrix [24], precise temperature control [24], and minimizing void formation during manufacturing [25], all of which can lead to nozzle clogging and inconsistent mechanical properties with reduced fabrication accuracy. In response to these challenges, SLA 3D printing has emerged as an alternative. Y. Sano et al. utilized SLA 3D printing to introduce a method for manufacturing short or continuous fiber composites, demonstrating a remarkable 7.2-fold increase in tensile strength compared to bulk resin specimens [25]. Similarly, S. Zang et al. [26] employed SLA 3D printing to produce lignin-reinforced composites, observing an enhancement in tensile strength ranging from 46% to 64% with the addition of lignin. Despite these promising findings, research on SLA-printed composites remains scarce.

Considering the information discussed above, it is evident that while both fiber treatment and extraction methods are crucial for enhancing the mechanical properties of composite materials, the feasibility of extracting bagasse fibers from sugarcane rind remains unexplored. Additionally, the recently emerged additive manufacturing, which presents itself as a viable alternative to traditional composite manufacturing methods, has not been thoroughly investigated. Therefore, the study's objective is to effectively use alkaline treated fiber from bagasse rind in the fabrication of a new class of bagasse-reinforced epoxy-based composite material through stereolithography (SLA) 3D printing.

2. Materials and Methods

2.1. Materials

The process of bagasse production is illustrated in Figure 1. For this study, bagasse generated during the sugarcane juice pressing was collected from local street vendors. It was then processed and used for subsequent bagasse fiber extraction and utilization in biocomposites. In the literature, though it has been noted that bagasse is typically sourced from sugar mills, no specific location of the stem to extract the bagasse fibers was mentioned. Therefore, in this research, we first extracted fibers directly from bagasse rinds. Subsequently, the properties of these fibers were evaluated.

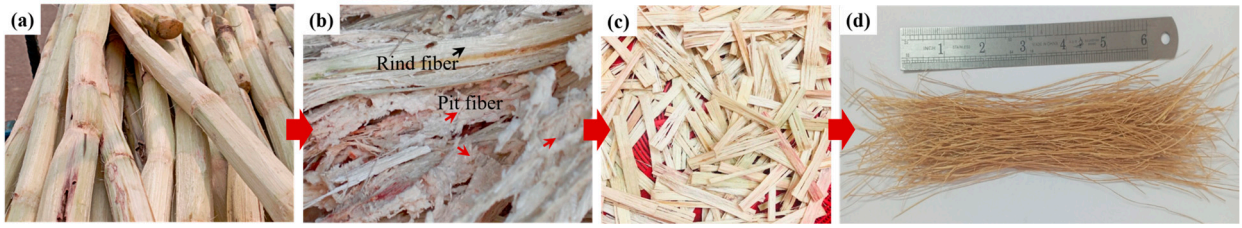

Figure 1. Steps of sugarcane bagasse fiber generation: (**a**) Cleaned chopped stems prepared for juice production, (**b**) sugarcane bagasse fibrous residue after juice extraction, (**c**) sugarcane rind fibers, and (**d**) sugarcane bagasse fiber obtained using chemical retting process.

In the present study, three different processing methods were used to extract the fibers from the rind. The fiber extraction methods are schematically shown in Figure 2. In the first process (Process-1), the initially collected bagasse underwent a thorough washing in running tap water and was subsequently dried outdoors under the sun for 72 h cumulatively over 12 days (6 h each day). Following the drying, the rind fibers were manually extracted and immersed in a 5 wt.% NaOH solution for 15 h. The resulting fine fibers were then extracted through combing operations. Next, the fibers underwent another round of washing with water and re-dried under the sun for an additional 72 h. In the second process (Process-2), the as-collected bagasse was washed thoroughly in running tap water and then dried under the sun for a total of 6 h. The rind fibers were then extracted manually and immersed in a 1 wt.% NaOH solution for 25 h. The resulting fine fibers were then extracted by combing operations. The fibers were then washed with water and dried under the sun for 72 h over 12 days. In the third process (Process-3), the as-collected bagasse was first soaked in water for 4 weeks. It was then washed thoroughly in running tap water and the rind fibers were manually collected from it. The collected rind fibers were then dried outdoors for 72 h (12 days) and subsequently immersed in a 1 wt.% NaOH solution for 18 h. The resulting fine fibers were then extracted by combing operations, which were then washed with water and dried outdoors for 72 h (12 days).

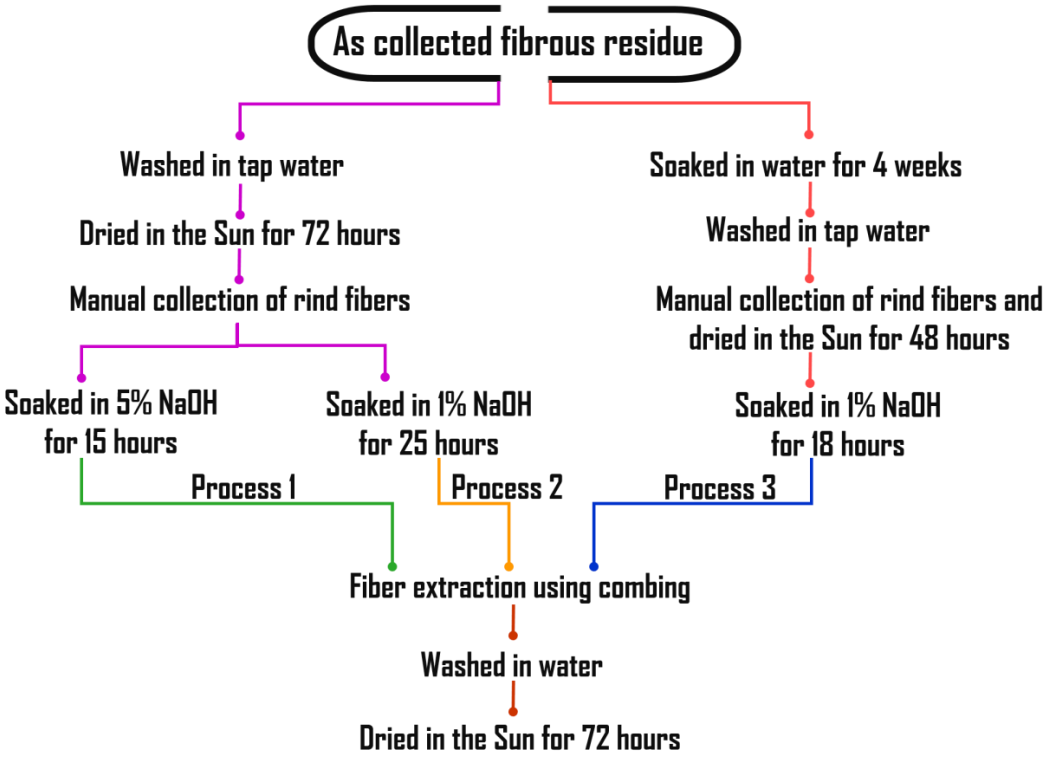

Figure 2. Flow chart highlighting the steps employed in the preparation of bagasse fiber.

2.2. FTIR Spectroscopy

FTIR spectra of the bagasse fibers were acquired using an Agilent Cary 630 spectrometer operating in attenuated total reflectance (ATR) mode. The measurements were conducted within a wavenumber range spanning from 500 cm^{-1} to 4000 cm^{-1}, at a spectral resolution of 8 cm^{-1}. Each spectrum was meticulously obtained through 32 scans to ensure robust data acquisition.

2.3. Fiber Diameter Measurement

Twenty fibers from each group (P1, P2, and P3) were randomly selected for observation under a Motic AE 2000 microscope. The microscope was outfitted with Motic Image Plus 3.0 software for image acquisition. Subsequently, the acquired images were imported into ImageJ version 1.53 g for fiber diameter measurements. It was assumed that the fibers were cylindrical in shape during measurement. To ensure accuracy, twenty different locations along the length of each fiber were randomly chosen, and their diameters were measured. The procedure for measuring fiber diameter is outlined elsewhere [27].

2.4. 3D Printer

Specimens for the present study were fabricated using the ANYCUBIC Photon M3 Max 3D printer machine with a *z*-axis accuracy of 0.01 mm. The machine can produce layers with thicknesses ranging from 0.01 to 0.15 mm. The geometry created in SolidWorks was converted to STL format, followed by slicing the layers using ANYCUBIC Photon Slicer software. The resin was cured by controlling a laser point with a wavelength of 405 nm based on the slice data. The ANYCUBIC Photon Slier software sets and manages key parameters.

2.5. Resin

A UV-curable standard photopolymer resin from Sonlu China was used as the matrix. The density and viscosity of the resin at 25 °C are 100–300 cps and 1.05–1.15 g/m^3, respectively. The curing wavelength of the resin is 405 nm.

2.6. Composite Fabrication Method

Tensile specimens in accordance with ASTM D638-type 4 standard (33 mm gauge length, 6 mm gauge width, and 3 mm thickness) were first designed in Solidworks as shown in Figure 3a. An STL (Stereolithography Interface Format) file of the tensile test specimen was then loaded into the Anycubic Photon 3D Slicer Software to generate the G code. A deposition layer height of 0.1 mm was chosen. The ANYCUBIC 3D printer subsequently interpreted the generated G code to create the desired part via layer-by-layer photocuring. After 50% layer formation, the 3D printer was paused. Then, 0.15 g of bagasse fibers were placed parallel to the loading direction and the printing was resumed to complete the specimen. Once complete, the specimen was removed from the build plate manually and soaked in an isopropyl alcohol bath to remove any unpolymerized resin on the outer surface. The cleaned samples were then cured using UV light for 15 min. A typical bagasse fiber-reinforced 3D-printed composite specimen is shown in Figure 3b.

As documented in Section 2.1, the fibers were extracted using three different processes: Process-1, Process-2, and Process-3. Hereinafter, composites prepared using fibers extracted through Process-1 are named Composite P1, those using fibers from Process-2 are named Composite P2, and those using fibers from Process-3 are named Composite P3.

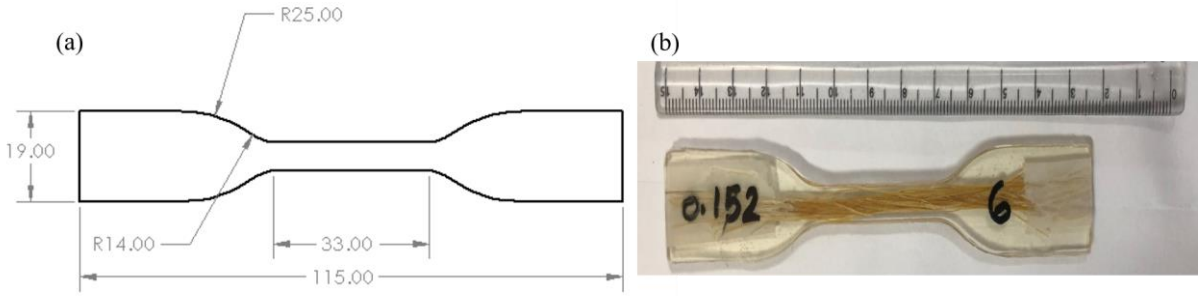

Figure 3. (**a**) Geometry and the dimension of the tensile test specimen (unit: mm). (**b**) Bagasse fiber-reinforced 3D-printed composite specimen.

2.7. Tensile Test

A single-fiber tensile test was conducted using a Titan Universal Tensile Testing machine equipped with a 200 N load cell, operating at a speed of 5 mm/min. From each group, twenty single-fibers were randomly selected and affixed to paper tabs prior to the test. Similarly, the tensile test for the composite material was performed using the same Titan Universal Tensile Testing machine but with a load cell capacity of 5 kN, maintaining a consistent test speed of 5 mm/min. Five specimens from each group were subjected to the tensile test. During testing, the load–displacement curve was recorded for analysis.

2.8. SEM

The fracture surfaces of specimens of the 3D-printed bagasse-reinforced composite material and 3D-printed resin samples were thoroughly examined using a scanning electron microscope (SEM).

3. Results

3.1. FTIR Analysis

The FTIR spectra of bagasse fibers produced in Process-1, Process-2, and Process-3 are depicted in Figure 4, alongside the FTIR spectra of rind fibers for comparison. The examination of Figure 4 reveals that the presence of an absorption band at 3335 cm^{-1} was associated with the O-H stretching mode of hydroxyl groups present in the cellulose [28]. The absorption peaks observed at 2925 cm^{-1} and 2851 cm^{-1} likely originate from the stretching vibrations of C-H bonds in CH_2 and CH_3 groups present in the cellulose, lignin, and hemicellulose [29]. It is present in both treated and untreated fibers. The peaks at 1730 cm^{-1} and 1632 cm^{-1} are associated with the stretching vibrations of non-conjugated carbonyl groups (C=O), primarily from hemicellulose and conjugate carbonyl found in lignin, respectively [30,31]. The absorption peak at 1422 cm^{-1} is due to the C=C vibration of the aromatic ring of lignin and hemicellulose, whereas the peak at 1244 cm^{-1} was attributed to out-of-plane C-O-C stretched aryl alkyl ethers of lignin [32]. The absorption peak at 1035 cm^{-1} corresponds to the vibration of the C-O bond. The absorption band around 898 or 832 cm^{-1} indicates the stretching vibration of glycosidic C-H bonds in cellulose molecules, particularly representing β-glycosidic bonds and the non-crystalline regions of cellulose [33].

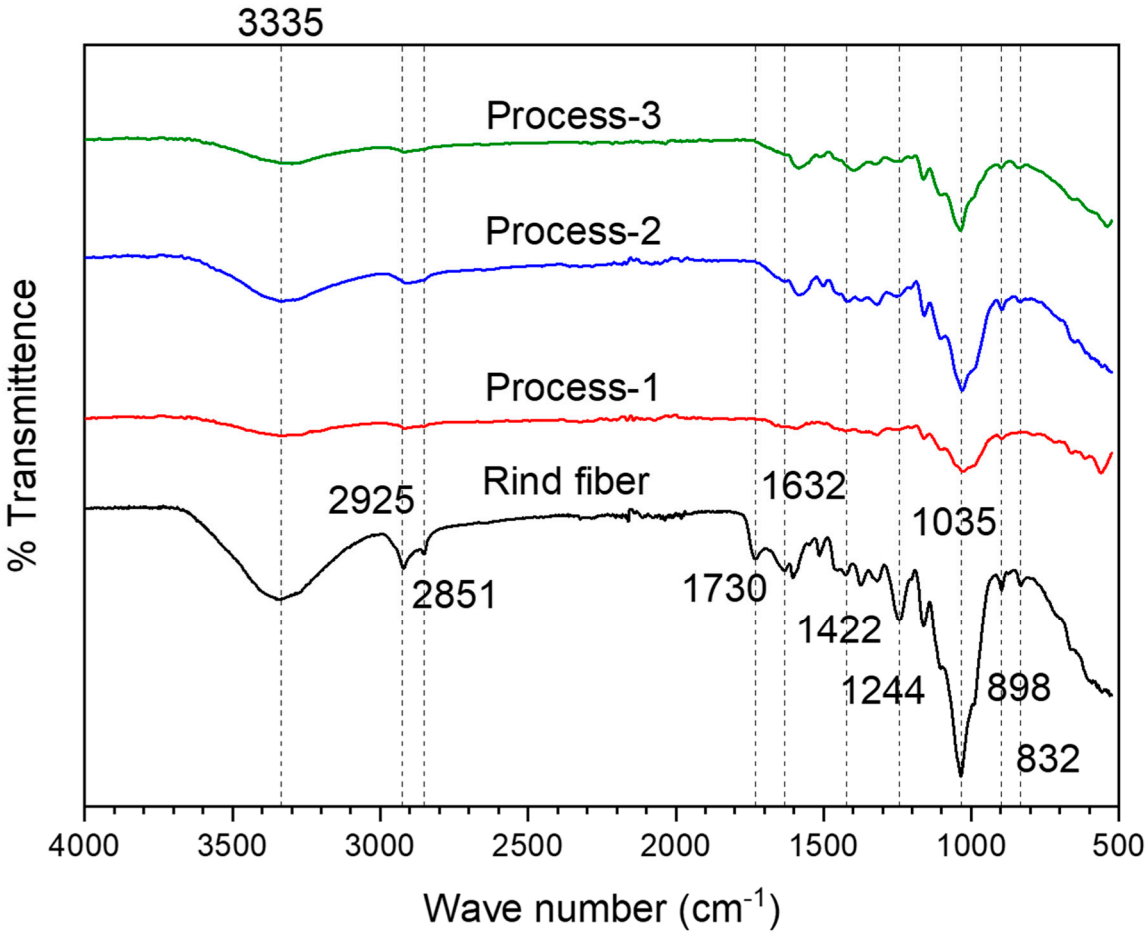

Figure 4. FTIR spectra of fibers.

3.2. Fiber Diameter

Figure 5 illustrates the distribution of diameters across the length of 20 randomly selected bagasse fibers for each process. The bagasse fibers exhibit significant diameter variation along their length, and the diameter distribution is skewed to the left. Furthermore, the diameters of bagasse fibers obtained using Process-1, Process-2, and Process-3 range from 210 to 903 µm, 120 to 642 µm, and 181 to 726 µm, respectively. The mean diameter of bagasse fibers was approximately 250 µm for P1, 425 µm for P2, and 360 µm for P3. Diameter distributions are often described by either a two-parameter Weibull distribution [34] or a log-normal distribution [35]. In this research, a log-normal distribution was chosen to fit the datasets.

The probability density function of a log-normal distribution is given by [36]:

$$f(x) = \frac{1}{x\sigma\sqrt{2\pi}} exp\left[-\frac{(\ln x - \mu)^2}{2\sigma^2}\right] \quad (1)$$

where μ and σ are the mean value and standard deviation, respectively, of the logarithm of the variable x, which is the fiber diameter.

As seen in the figure, the distribution of fiber diameters for all processes can be modeled using a log-normal distribution. The bagasse fibers in the present study showed a unimodal log-normal distribution.

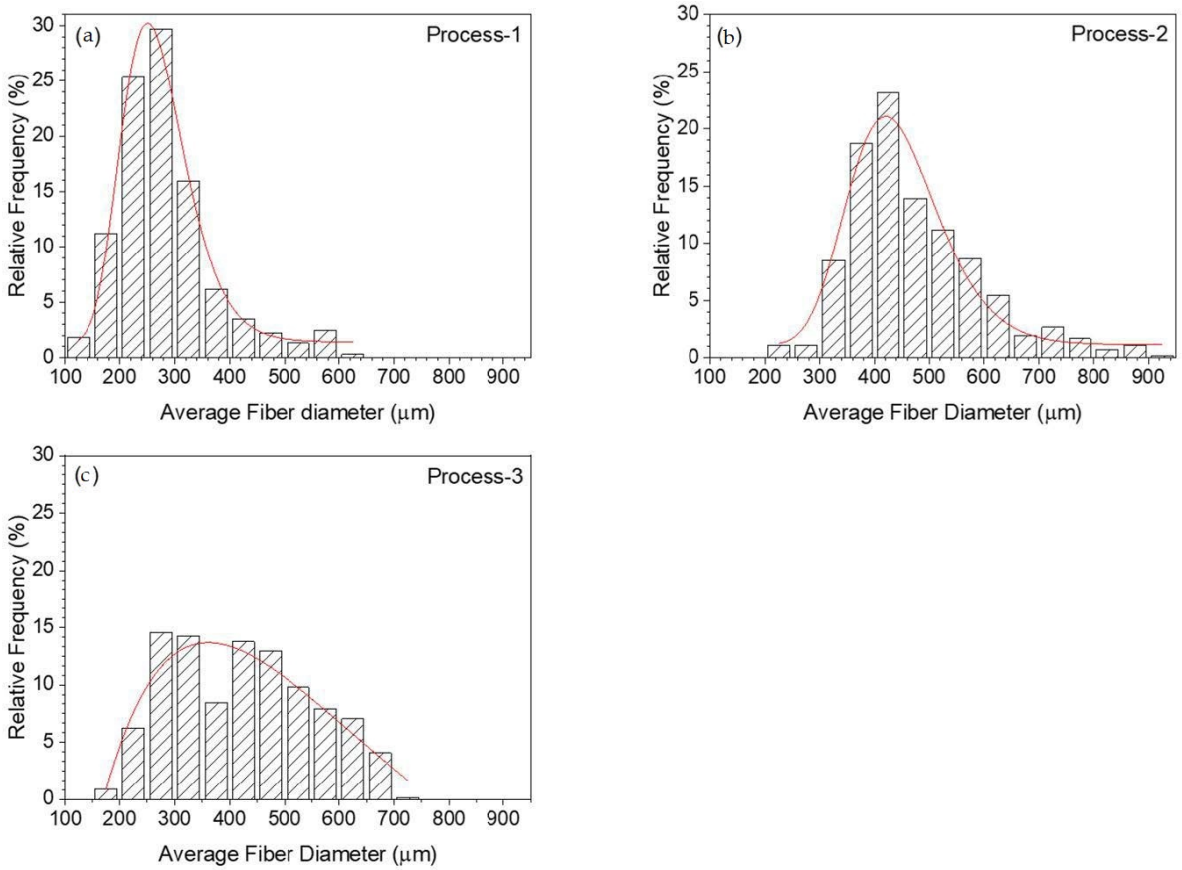

Figure 5. Histogram illustrating the variation in diameter of bagasse fibers extracted through (**a**) Process-1; (**b**) Process-2; and (**c**) Process-3.

3.3. Fiber Strength

Figure 6 displays a typical load versus elongation curve for bagasse fiber. Initially, the bagasse fibers demonstrate a linear elastic behavior, followed by abrupt failure without noticeable plastic deformation. Other fibers, like bamboo fibers, display a similar load-versus-elongation profile [37]. The detailed tensile results of the bagasse fibers are summarized in Table 1. Based on Table 1 and Figure 6, it is evident that bagasse fibers extracted using Process-1 exhibited the highest average tensile strength (5.9 N). This strength is approximately 90% higher than that of bagasse fibers obtained using Process-3 and about 78% higher than that of bagasse fibers obtained using Process-2.

Table 1. Tensile results of bagasse fiber.

Material	Average Breaking Load (N)
Process-1	5.9 ± 2.4
Process-2	3.3 ± 1.3
Process-3	3.1 ± 1.4

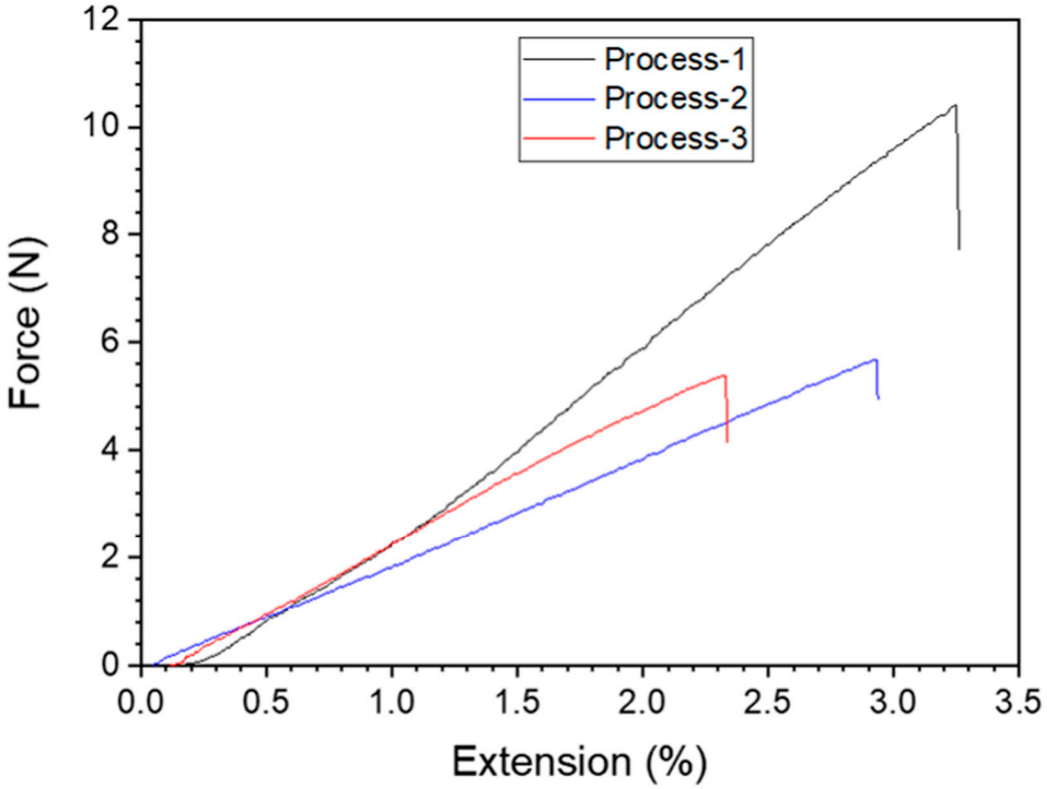

Figure 6. Representative load-versus-displacement curve for fiber.

Table 1 also reveals that the tensile strength of bagasse fiber varies significantly with the variation of standard deviation values. This variation highlights the limitations of deterministic models in fully characterizing the tensile properties of bagasse fibers. Therefore, utilizing a statistical model is more suitable for explaining such variability, rather than relying solely on average tensile strength and standard deviation. In recent years, Weibull statistics [38] have garnered significant attention for predicting the scatter characteristics of the tensile properties of both fibers and fiber-reinforced polymer composites [39,40]. The tensile strength distribution can be accurately modeled using the two-parameter Weibull distribution [40,41]. Therefore, in the present study, the scatter of tensile strength of bagasse fibers is analyzed using the two-parameter Weibull distribution. The detailed equations and their meanings can be found in Ref. [27].

Figure 7a shows the two-parameter Weibull plots generated using least-squares minimization. The calculated values of the shape parameter and the characteristic breaking load are presented in Table 2. In each instance, a strong linear relationship was observed, with R^2 values between 0.94 and 0.96, indicating that the experimental data can be effectively described by the two-parameter Weibull distribution equation. The Weibull modulus for natural fibers typically ranges from 1 to 6. The results in Table 3 align with this range, comparable to those for jute [42] and palm fiber [43]. From Table 2, the highest Weibull modulus (α) observed for bagasse fibers obtained through Process-2 indicates that these fibers are more likely to fracture compared to those from Process-1 and Process-3. The bagasse fibers extracted via Process-1 showed the highest scale parameter of 6.8 N, with a 63% probability of failure. In comparison, fibers obtained through Process-2 and Process-3 reached the same probability of failure at approximately only half of this strength.

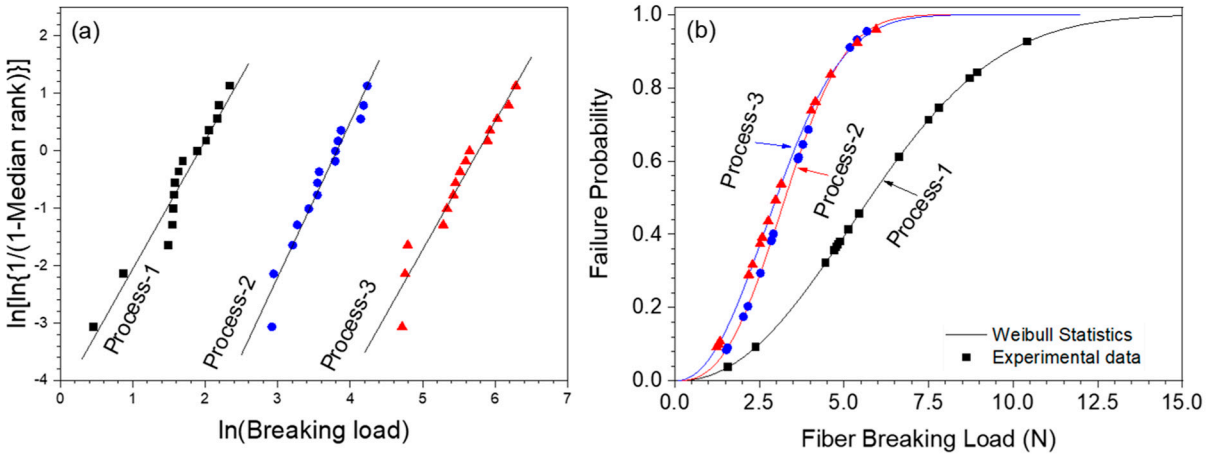

Figure 7. (**a**) Two-parameter Weibull plot of the tensile breaking load of bagasse fibers obtained from different processing methods. (**b**) Failure probability of bagasse fibers obtained from different processing methods.

Table 2. Weibull modulus (α), scale parameter (σ_0), and correlation coefficient (R^2) of the two-parameter Weibull distribution equation (obtained from Figure 6).

Material	Weibull Modulus (α)	Constant Term (c)	Scale Parameter (σ_0)	Precision Adjustment (R^2)
Process-1	2.24	−4.3	6.80	0.94
Process-2	2.7	−3.56	3.74	0.96
Process-3	2.24	−2.83	3.53	0.94

Table 3. Tensile results of 3D-printed bagasse-reinforced composite.

Material	Ultimate Tensile Strength (MPa)	% Improvement
Resin	20.4 ± 1.7	
Composite P1	34.5 ± 2.9	69.3%
Composite P2	31.6 ± 3.2	55%
Composite P3	32.8 ± 2.9	61%

Figure 7b shows the theoretical strength distribution alongside the experimental failure probability results, indicating a strong correlation with the tensile load distribution. The tensile load needed for a 95% probability of rupture is about 11 N for bagasse fibers extracted by Process-1, 5.9 N for those extracted by Process-2, and 5.5 N for fibers extracted by Process-3.

3.4. Composite Tensile Strength

Figure 8 shows the typical force-versus-extension curves for the 3D-printed bagasse-reinforced composite material. For comparison, the force-versus-extension curve for the 3D-printed standard resin is also shown in Figure 7. In all cases, the maximum load was observed just before the failure of the specimen. The average tensile strength of the 3D-printed resin and 3D-printed bagasse-reinforced composite materials is tabulated in Table 2. It can be seen from Table 2 that the 3D-printed resin samples (without fill) exhibited an average ultimate tensile strength of 20.4 MPa with a standard deviation of 1.7 MPa. Remarkably, a significant enhancement in tensile strength was observed for the 3D-printed bagasse-reinforced composite material. The 3D-printed bagasse-reinforced composite

materials showed an average tensile strength of 34.5 MPa with a standard deviation of 2.9 MPa for Composite P1, 31.6 MPa with a standard deviation of 3.2 MPa for Composite P2, and 32.8 MPa with a standard deviation of 2.9 MPa for Composite P3, respectively.

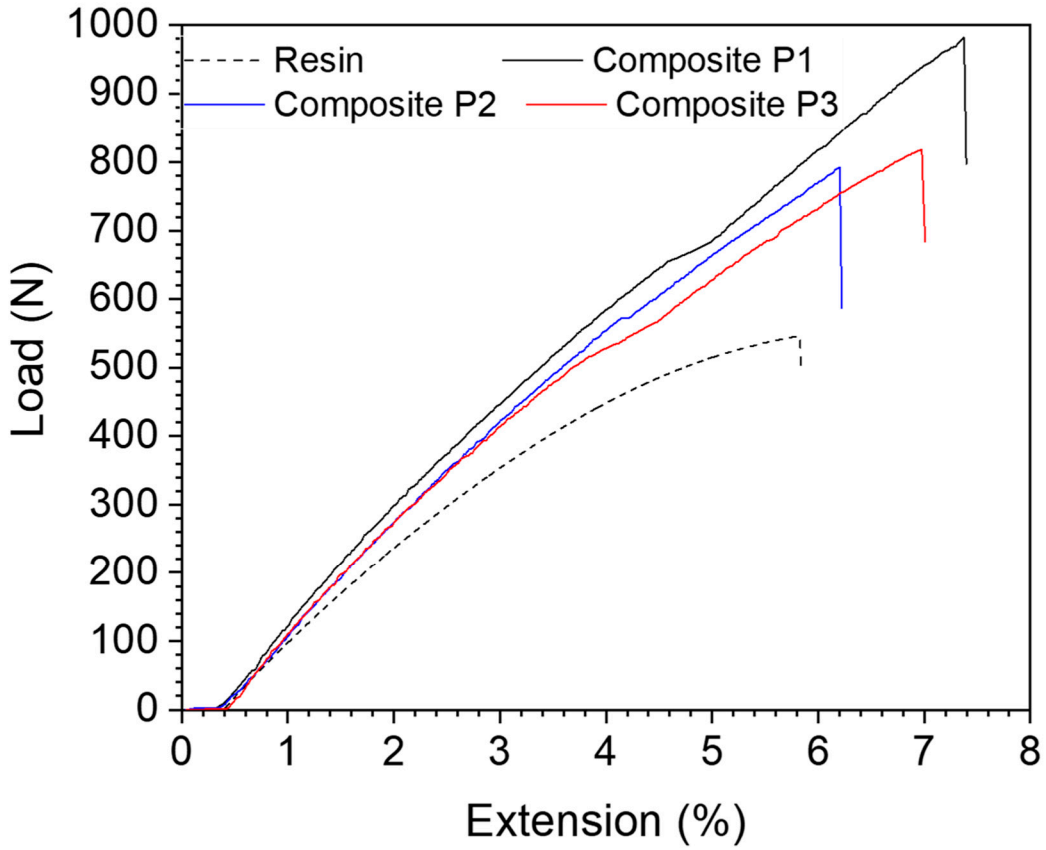

Figure 8. Load-versus-displacement curve for bagasse fiber-reinforced composite.

The effect of the addition of bagasse fiber as filler material on the tensile strength is evaluated using the "improvement rate", which is defined as:

$$\%\text{Improvement rate} = \frac{\sigma_{UTS,C} - \sigma_{UTS,R}}{\sigma_{UTS,R}} \times 100 \quad (2)$$

where $\sigma_{UTS,C}$ is the ultimate tensile strength of the 3D-printed jute-reinforced composite and $\sigma_{UTS,R}$ is the ultimate tensile strength of resin material.

As can be seen from Table 3, Composite P1 showed about 69% improvement in tensile strength, whereas Composite P2 showed about 55% improvement in tensile strength and Composite P3 showed about 61% improvement in tensile strength.

3.5. SEM

A sample of a 3D-printed bagasse fiber-reinforced composite specimen was cut along the fiber-loading direction, and the fiber–matrix interface was observed under SEM. A representative SEM micrograph is shown in Figure 9. The image indicates good adhesion between the bagasse fibers and the matrix. However, a closer inspection reveals some interfacial deboning at the interface.

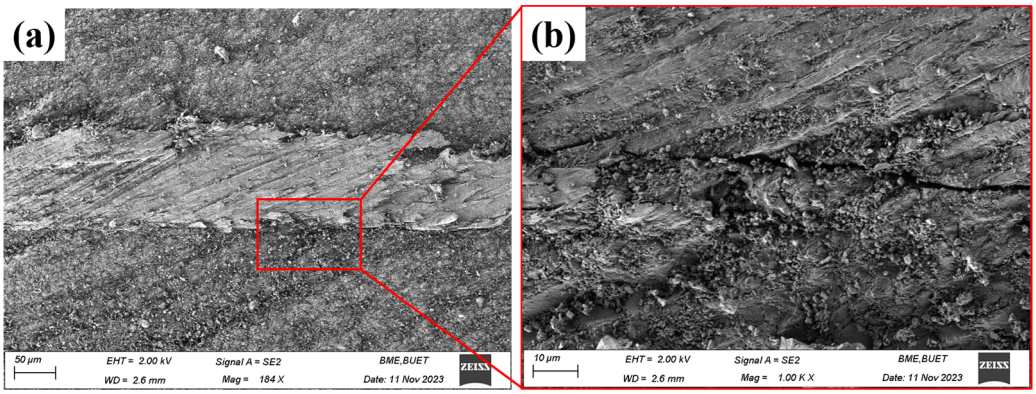

Figure 9. (**a**) SEM images showing the fiber–matrix interface of 3D-printed bagasse-reinforced composite; (**b**) magnified view of the part outlined by red rectangle in (**a**).

Figure 10 depicts a typical fracture zone of a 3D-printed bagasse fiber-reinforced composite under tension. Figure 10a,b shows that the tensile fracture surface of the 3D-printed resin material features numerous river-like cracks, which reveal its characteristic brittle-plastic nature with poor resistance to cracking and crack propagation [44]. As a result, the resin undergoes tensile fracture at a relatively low energy. However, in the fiber–matrix region, fiber breakage is clearly visible (Figure 10c). The reinforced bagasse fibers were difficult to pull out, leading to fiber breakage, particularly at the center of the specimen. Additionally, a fibrillation process occurred, consuming some of the energy among the elementary fibers (Figure 10d). Overall, fiber breakage and matrix cracks were predominant in the composites.

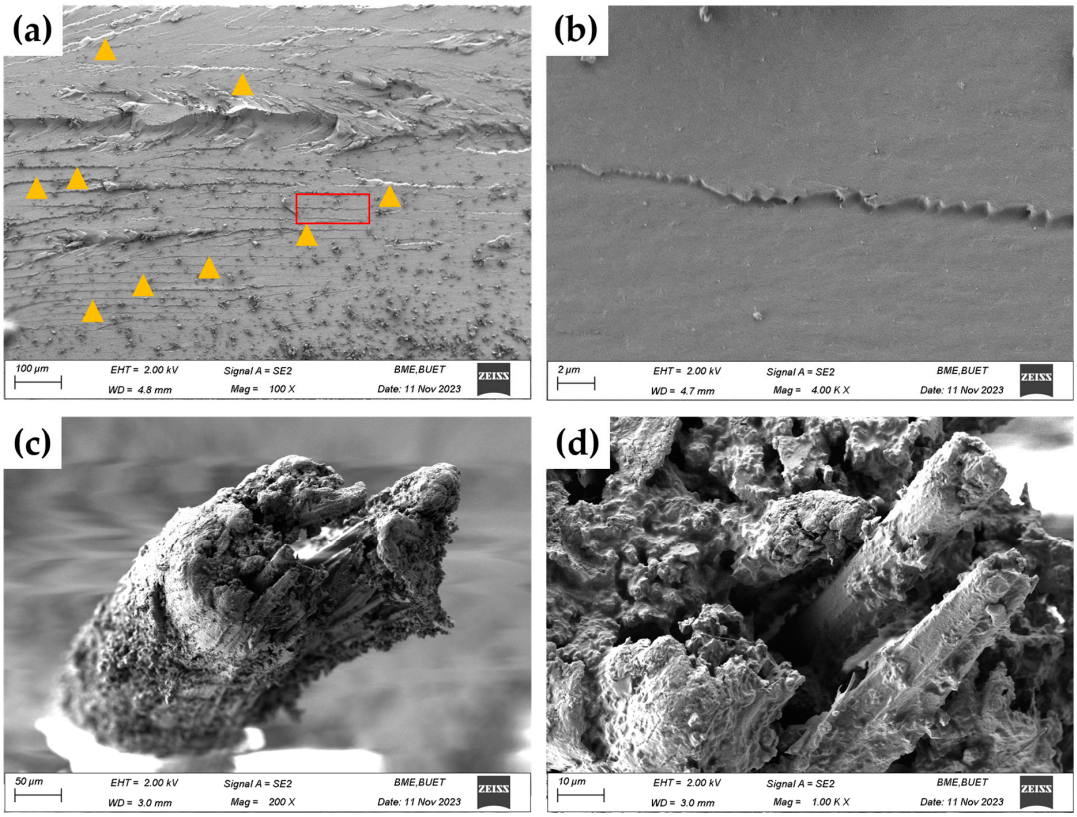

Figure 10. SEM images of the fracture surface of 3D-printed bagasse fiber-reinforced composite under tension showing (**a**) fracture of resin material; (**b**) magnified image of river-like line shown in (**a**) outlined by red rectangle; (**c**) fiber breakage; and (**d**) fibrillation of fiber.

3.6. Comparative Study

Figure 11 presents a comparison between the ultimate tensile strength of bagasse fiber-reinforced composite material fabricated using conventional methods like hand layup, injection molding, compression molding, and extrusion and the current study's findings on 3D-printed bagasse-reinforced composite material, drawing upon literature data. The synergistic effect of the fiber extraction process and the application of 3D printing technology in composite fabrication resulted in a dramatic improvement in tensile properties. Given that only a 2% volume fraction of bagasse fiber was used, it can be inferred that increasing the volume fraction would further enhance the tensile strength and overall performance of the composite.

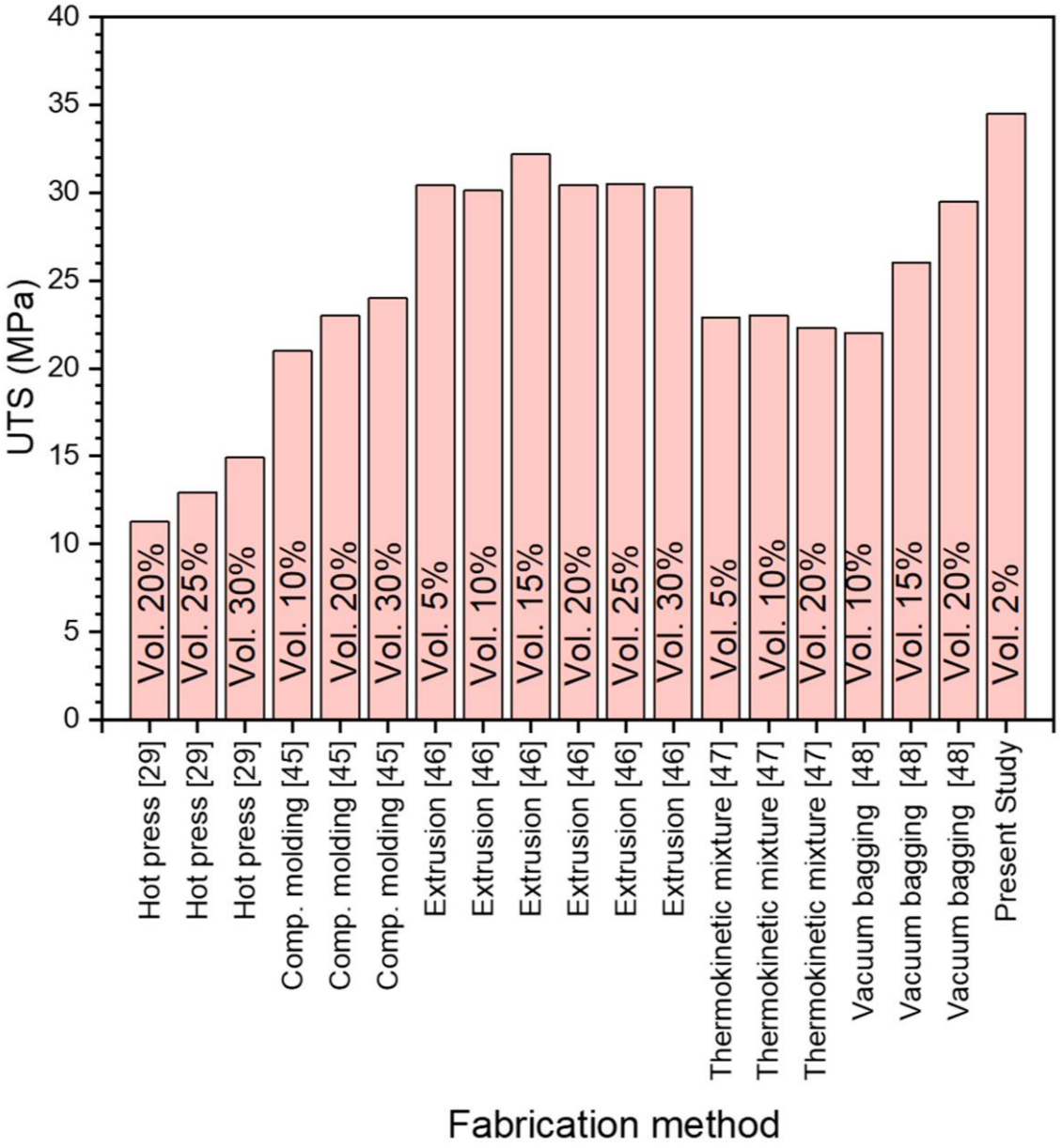

Figure 11. Comparison of ultimate tensile strength of 3D-printed bagasse-reinforced composites with literature data. Figure drawn based on data from Refs. [29,45–48].

4. Discussion

In fiber-reinforced composite materials, the fibers generally exhibit higher strength than the polymer matrix, leading to an improvement in the matrix's mechanical perfor-

mance when fibers are added. The primary roles of the fibers in fiber-reinforced composite materials include (i) bearing the majority of the tensile or compressive load applied to the composite and (ii) bridging matrix cracks and mitigating crack propagation by dissipating energy near the crack tips. While numerous studies have been conducted on bagasse-reinforced composite materials, there is a lack of in-depth analyses of bagasse fiber extraction and its mechanical performance, including its mechanical properties. Therefore, this study first focused on developing a fiber extraction method aimed at enhancing the material's sustainability. The properties of the obtained bagasse fibers were extensively evaluated, with a primary focus on functional group analysis, diameter measurement, and tensile strength assessment. Functional group analysis (Figure 3) revealed that both the concentration of NaOH and soaking time affected the presence of lignin and hemicellulose in the rind fibers. The peaks linked to the structure of lignin and hemicellulose decreased and, in some cases, completely disappeared. For instance, the absorption peaks at 2851 cm^{-1} and 1730 cm^{-1} were no longer apparent in Process-1, Process-2, and Process-3, respectively, suggesting that some lignin and hemicellulose were eliminated from the rind fibers. The C=C vibration of the aromatic ring of lignin around 1422 cm^{-1} decreased whereas the C-O-C stretched alkyl ethers around 1244 cm^{-1} completely disappeared for the extracted bagasse fibers. The outcome of the spectra illustrates that due to the soaking of the rind fibers in NaOH solution, the binding components such as hemicellulose, lignin, and amorphous cellulose were partially or completely dissolved, whereas the cellulose portion was not significantly affected. Marques et al. [49] also reported similar findings.

The diameter of bagasse fibers showed significant variation both between individual fibers and within the same fiber (Figure 5). Comparable diameter fluctuations have been noted in other natural fibers, including bamboo [37], sisal [50], and jute [51]. On the other hand, strength tests of bagasse fibers revealed a wide variation in breaking strength (Table 1). These variations can be ascribed to several factors, including fiber diameter, gauge length, and fiber fracture mechanisms. Additionally, factors such as origin, plant quality, weather, age, soil, and fiber extraction methods were also used to control the mechanical properties [27]. Monteiro et al. [52] reported that fibers with larger diameters break at lower stress compared to thinner fibers. During tensile deformation, the least strong fibrils within thicker fibers break at lower stress levels. Once weak fibril fractures, it initiates a defect in the fiber structure that spreads in a brittle manner until the fiber completely breaks. Moreover, studies have indicated a negative correlation between fiber strength and gauge length [53–55]. Additionally, with an increase in fiber gauge length, there is an increase in flaw distribution, enhancing the likelihood of the presence of a significant flaw. This results in stress localization and consequently reduces fiber strength. Conversely, cellulose significantly boosts tensile strength and Young's modulus, while lignin content has the opposite impact [56]. As depicted in Table 1, bagasse fibers extracted through Process-1 display the highest average tensile load, approximately 78% higher than those from Process-2, and 90% higher than those obtained using Process-3. Based on the information shown in Figures 4 and 5, it can be speculated that the synergistic effect of natural conditions, fiber extraction method, and fiber fracture mechanism created localized conditions conducive to fracture, resulting in considerable data scatter.

According to composite matrix theory, the tensile strength of natural fiber-reinforced polymer composites is highly dependent on the tensile strength of the fibers used [7]. Our findings revealed that bagasse fibers extracted using Process-1 exhibited the highest tensile strength. Consequently, 3D-printed composites reinforced with these fibers showed the highest (approximately 70%) improvement in tensile strength compared to specimens made from pure resin (Figure 8 and Table 3).

The load-bearing capacity of fiber-reinforced composites depends on (i) manufacturing defects such as voids [18] and (ii) local deformation processes such as fiber debonding or pullout, fiber fracture, etc. [57,58]. The presence of voids diminishes the performance of composites under service load by acting as stress concentration points, promoting further damage growth and leading to strength degradation. Therefore, minimizing porosity levels

is crucial for maintaining the performance of fiber-reinforced composite structures. On the other hand, the local deformation processes strongly depend on the interfacial adhesion between the fiber and the matrix. Strong interfacial adhesion led to fiber fracture, whereas poor interfacial adhesion resulted in fiber pullouts. The relatively better interfacial adhesion between the fiber and the matrix (Figure 9) and the observable fiber fracture phenomena (Figure 10) clearly indicate that 3D printing technology effectively enhances the quality of fiber–matrix interfacial bonding, consequently resulting in improved tensile properties of the composites.

The 3D-printed composites reinforced with bagasse fiber have showcased impressive tensile properties and provided solutions to the limitations of traditional composite manufacturing methods. This sets the stage for developing innovative composite materials that combine natural fibers with cutting-edge fabrication techniques, offering a promising path to tackle present and future economic and ecological challenges. Moreover, refining the quality of bagasse fiber through chemical extraction processes has the potential to revolutionize commercialization endeavors.

5. Conclusions

This study commenced by extracting bagasse fibers from sugarcane rind fibers through immersion in NaOH solutions of varying concentrations and durations. The ensuing bagasse fibers underwent a comprehensive property assessment. Subsequently, these fibers were employed in the production of composite materials via the 3D SLA printing technique. From this study, the following conclusions can be inferred:

- The outcome of the FTIR spectra illustrates that due to the soaking of the rind fibers in NaOH solution, the binding components such as hemicellulose, lignin, and amorphous cellulose were partially or completely dissolved, indicating that the cellulose portion was increased.
- The bagasse fibers extracted through Process-1 showed the highest average tensile load, approximately 78% higher than those from Process-2 and 90% greater than those obtained using Process-3. It is speculated that the synergistic interaction of thin bagasse fibers, along with the fiber fracture mechanism and elevated cellulose content, creates localized conditions for fracture and improved tensile load.
- 3D-printed composites reinforced with bagasse fibers extracted through Process-1 showed the highest improvement in tensile strength (approximately 70%) compared to specimens made from pure resin. The lack of pores in the composite and the observable fiber fracture phenomena clearly indicate that 3D printing technology effectively enhances the quality of fiber–matrix interfacial bonding, consequently resulting in improved tensile properties of the composites.

The method that was used to fabricate bagasse-reinforced composite material extends the potential of stereolithography (SLA) 3D printing to produce load-bearing components, which is not achievable with traditional manufacturing techniques. Future research will address aspects not considered in this study, such as the impact of fiber volume fraction on mechanical properties (including tensile, flexural, and impact resistance), water absorption characteristics, and the influence of environmental factors on the mechanical properties of the composites. The application of modeling and simulation tools can also minimize experimental testing for optimum parameter selection for fiber extraction as well as additive processing. Moreover, improved numerical models are necessary to comprehend the deformation and failure mechanisms of the composite under mechanical and thermal loads.

Another aspect of improvement lies in the domain of composite processing for high-quality and consistent production. Future direction should either focus on developing new technologies or upgrading the current SLA 3D printing process. For example, incorporating robotic additive manufacturing can ensure seamless fiber integration to increase consistency and productivity, resulting in parts with superior quality. The progress in vision systems offers new possibilities for integrated systems that allow robots to adjust their functions in real time based on their surroundings. Additionally, integrating artificial intelligence into

robotic systems can help develop smart additive manufacturing processes with optimized production flow for enhanced quality and superior properties of the products.

Author Contributions: Conceptualization, M.S.B.; methodology, M.S.B., M.A.R. and A.M.; formal analysis, A.M. and M.A.R.; investigation, A.M. and R.I.; writing—M.S.B. and A.F.; writing—review and editing, M.K., M.E.K., M.R.H. and M.A.R.; supervision, M.S.B.; funding acquisition, M.S.B. and M.K. All authors have read and agreed to the published version of the manuscript.

Funding: This research was funded by Ahsanullah University of Science and Technology (AUST), grant number ARP/2022/MPE/03/08.

Data Availability Statement: The original contributions presented in this study are included in this article; further inquiries can be directed to the corresponding author.

Conflicts of Interest: The authors declare no conflicts of interest. The funders had no role in the design of the study; in the collection, analyses, or interpretation of data; in the writing of the manuscript; or in the decision to publish the results.

References

1. Zheng, H.; Zhang, W.; Li, B.; Zhu, J.; Wang, C.; Song, G.; Wu, G.; Yang, X.; Huang, Y.; Ma, L. Recent advances of interphases in carbon fiber-reinforced polymer composites: A review. *Compos. Part B* **2022**, *233*, 109639. [CrossRef]
2. Olszewski, A.; Kosmela, P.; Mielewczyk-Gryń, A.; Piszczyk, Ł. Bio-Based Polyurethane Composites and Hybrid Composites Containing a New Type of Bio-Polyol and Addition of Natural and Synthetic Fibers. *Materials* **2020**, *13*, 2028. [CrossRef] [PubMed]
3. Kirmasha, Y.K.; Sharba, M.J.; Leman, Z.; Sultan, M.T.H. Mechanical Performance of Unstitched and Silk Fiber-Stitched Woven Kenaf Fiber-Reinforced Epoxy Composites. *Materials* **2020**, *13*, 4801. [CrossRef]
4. Singh, T.; Gangil, B.; Patnaik, A.; Biswas, D.; Fekete, G. Agriculture waste reinforced cornstarch-based biocomposites: Effect of rice husk/walnut shell on physicomechanical, biodegradable and thermal properties. *Mater. Res. Express* **2019**, *6*, 045702. [CrossRef]
5. Prasad, V.; Vijayyakumar, A.A.; Jose, T.; George, S.C. A comprehensive Review of Sustainability in Natural-Fiber Reinforced Polymers. *Sustainability* **2024**, *16*, 1223. [CrossRef]
6. Satyanarayana, K.G.; Guimaraes, J.L.; Wypych, F. Studies on Lignocellulosic fibers of Brazil. Part 1: Source, production morphology, properties and applications. *Compos. A Appl. Sci. Manuf.* **2007**, *38*, 1694–1709. [CrossRef]
7. Ku, H.; Wang, H.; Pattarachaiyakoop, M.; Trada, M. A review on the tensile properties of Natural fiber reinforced polymer composites. *Compos. B Eng.* **2011**, *42*, 856–873. [CrossRef]
8. Mushtaq, B.; Ahmad, S.; Ahmad, F.; Nawab, Y. Alternative natural fibers for biocomposites. In *Natural Fibers to Composites: Process, Properties, Structures*; Springer International Publishing: Cham, Switzerland, 2022; pp. 1–18.
9. Siakeng, R.; Jawaid, M.; Ariffin, H.; Sapuan, S.M.; Asim, M.; Saba, N. Natural fiber reinforced polylactic acid composites: A review. *Polym. Compos.* **2019**, *40*, 446–463. [CrossRef]
10. Shaker, K.; Nawab, Y.; Jabbar, M. Bio-Composites: Eco-Friendly Substitute of Glass Fiber Composites. In *Handbook of Nanomaterials and Nanocomposites for Energy and Environmental Applications*; Springer: Cham, Switzerland, 2020; pp. 1–25.
11. Verma, D.; Gope, P.C.; Maheshwari, M.K.; Sharma, R.K. Bagasse Fiber Composites—A Review. *J. Mater. Environ. Sci.* **2012**, *3*, 1079–1092.
12. Pandey, A.; Soccol, C.R.; Nigam, P.; Soccol, V.T. Biotechnological potential of agro-industrial residues. I: Sugarcane bagasse. *Bioresour. Technol.* **2000**, *74*, 69–80. [CrossRef]
13. Bilba, K.; Arsène, M. Silane treatment of bagasse fibre for reinforcement of cementitious composites. *Compos. Part A Appl. Sci. Manuf.* **2008**, *39*, 1488–1495. [CrossRef]
14. Candido, R.G.; Godoy, G.G.; Gonsalves, A.R. Study of sugarcane bagasse pretreatment with sulfuric acid as a step of cellulose obtaining. *Int. J. Nutr.* **2012**, *6*, 6–10.
15. Lopez, R.; Poblano, V.M.; Licea-Clavere, A.; Avalos, M.; Alvarez-Castillo, A.; Castano, V.M. Alkaline surface modification of sugarcane bagasse. *Adv. Compos. Mater.* **2012**, *9*, 99–108. [CrossRef]
16. Wirawan, R.; Sapuan, S.M.; Yunus, R.; Abdan, K. Properties of sugarcane bagasse poly (vinyl chloride) composites after various treatments. *J. Compos. Mater.* **2011**, *45*, 1667–1674. [CrossRef]
17. Sathish, S.; Karthi, N.; Prabhu, L.; Gokulkumar, S.; Balaji, D.; Vigneshkumar, N.; Dinesh, V.P. A review of natural fiber composites: Extraction methods, chemical treatments and applications. *Mater. Today Proc.* **2021**, *45*, 8017–8023. [CrossRef]
18. Mehdikhani, M.; Gorbatikh, L.; Verpoest, I.; Lomov, S.V. Voids in fiber-reinforced polymer composites: A review on their formation, characteristics, and effects on mechanical performance. *J. Compos. Mater.* **2019**, *53*, 1579–1669. [CrossRef]
19. Devadiga, D.G.; Subrahmanya Bhat, K.; Mahesha, G.T. Sugarcane bagasse fiber reinforced composites: Recent advances and applications. *Cogent Eng.* **2020**, *7*, 1823159. [CrossRef]
20. Rajendran Royan, N.R.; Leong, J.S.; Chan, W.N.; Tan, J.R.; Shamsuddin, Z.S.B. Current State and Challenges of Natural Fibre-Reinforced Polymer Composites as Feeder in FDM-Based 3D Printing. *Polymers* **2021**, *13*, 2289. [CrossRef]

21. Mohan, N.; Senthil, P.; Vinodh, S.; Jayanth, N. A review on composite materials and process parameters optimization for the fused deposition modelling process. *Virtual Phys. Prototyp.* **2017**, *12*, 47–59. [CrossRef]
22. Mazzanti, V.; Malagutti, L.; Mollica, F. FDM 3D printing of polymers containing natural fillers: A review of their mechanical properties. *Polymers* **2019**, *11*, 1094. [CrossRef] [PubMed]
23. Moran, J.; Alvarez, V.; Petrucci, R.; Kenny, J.; Vazquez, A. Mechanical properties of polypropylene composites based on natural fibers subjected to multiple extrusion cycles. *J. Appl. Polym. Sci.* **2007**, *103*, 228–237. [CrossRef]
24. Van den Oever, M.J.A.; Beck, B.; Müssig, J. Agrofibre reinforced poly (lactic acid) composites: Effect of moisture on degradation and mechanical properties. *Compos. Part A Appl. Sci. Manuf.* **2010**, *41*, 1628–1635. [CrossRef]
25. Sano, Y.; Matsuzaki, R.; Ueda, M.; Todoroki, A.; Hirano, Y. 3D printing of discontinuous and continuous fiber composites using stereolithography. *Addit. Manuf.* **2018**, *24*, 521–527.
26. Zhang, S.; Li, M.; Hao, N.; Ragauska, A.J. Stereolithography 3D printing of Lignin Reinforced Composites with Enhanced Mechanical Properties. *ACS Omega* **2019**, *4*, 20197–20204. [CrossRef]
27. Bhuiyan, M.S.; Rahman, M.A.; Farabi, M.S.; Hasan, M.M. Tensile behavior of geometrically irregular bagasse fiber. *Appl. Mech.* **2021**, *2*, 274–288. [CrossRef]
28. Corrales, R.C.N.R.; Mendes, F.M.T.; Perrone, C.C.; Anna, C.S.; de Souza, W.; Abud, Y.; Bon, E.P.S.; Ferreira-Leitão, V. Structural evaluation of sugarcane bagasse steam pretreated in the presence of CO_2 and SO_2. *Biotechnol. Biofuels* **2012**, *5*, 36. [CrossRef]
29. Anggono, J.; Sugondo, S.; Sewucipto, S.; Purwaningsih, H.; Henrico, S. The use of sugarcane bagasse in PP matrix composites: A comparative study of Bagasse treatment using Calcium Hydroxide and Sodium Hydroxide on composite strength. *AIP Conf. Proc.* **2017**, *1788*, 030055.
30. Biagiotti, J.; Puglia, D.; Torre, L.; Kenny, M.J.; Arbelaiz, A.; Cantero, G.; Marieta, C.; Llano-Ponte, R.; Mondragon, I. A systematic investigation on the influence of the chemical treatment of natural fibers on the properties of their polymer matrix composites. *Polym. Compos.* **2004**, *25*, 470–479. [CrossRef]
31. Liu, W.; Mohanty, A.K.; Drzal, L.T.; Askel, P.; Misra, M. Effect of alkali treatment on the structure, morphology and thermal properties of native grass fibers as reinforcements for polymer matrix composites. *J. Mater. Sci.* **2004**, *39*, 1051–1054. [CrossRef]
32. Costa, L.A.S.; Assis, D.J.; Gomes, G.V.P.; Silva, J.B.; Fonsêca, A.F.; Druzian, J.I. Extraction and characterization of nanocellulose from corn stover. *Mater. Today Proc.* **2015**, *2*, 287–294. [CrossRef]
33. Bian, J.; Peng, F.; Peng, X.P.; Xiao, X.; Peng, P.; Xu, F.; Sun, R.C. Effect of [Emim]Ac pretreatment on the structure and enzymatic hydrolysis of sugarcane bagasse cellulose. *Carbohydr. Polym.* **2014**, *100*, 211–217. [CrossRef] [PubMed]
34. Fu, S.Y.; Lauke, B. Effects of fibre length and orientation distributions on the tensile strength of short-fibre-reinforced polymers. *Compos. Sci. Technol.* **1996**, *56*, 1179–1190. [CrossRef]
35. Jiang, B.; Liu, C.; Zhang, C.; Wang, B.; Wang, Z. The effect of non-symmetric distribution of fiber orientation and aspect ratio on elastic properties of composites. *Compos. B Eng.* **2007**, *38*, 24–34. [CrossRef]
36. Le Moigne, N.; van den Oever, M.; Budtova, T. A statistical analysis of fiber size and shape distribution after compounding in composites reinforced by natural fibers. *Compos. Part A Appl. Sci. Manuf.* **2011**, *42*, 1542–1550. [CrossRef]
37. Trujillo, E.; Moesen, M.; Osorio, L.; Van Vuure, A.W.; Ivens, J.; Verpoest, I. Bamboo fibers for reinforcement in composite materials: Strength Weibull analysis. Compos. *Part A Appl. Sci. Manuf.* **2014**, *61*, 115–125. [CrossRef]
38. Weibull, W. A statistical function of wide applicability. *J. Appl. Mech.* **1951**, *18*, 293–307. [CrossRef]
39. Barbero, E.; Fernández-Sáez, J.; Navarro, C. Statistical analysis of the mechanical properties of composite materials. *Compos. B Eng.* **2000**, *31*, 375–381. [CrossRef]
40. Swolfs, Y.; Morton, H.; Scott, A.E.; Gorbatikh, L.; Reed, P.A.S.; Sinclair, I.; Spearing, S.M.; Verpoest, I. Synchrotron radiation computed tomography for experimental validation of a tensile strength model for unidirectional fibre-reinforced composites. *Compos. Part A Appl. Sci. Manuf.* **2015**, *77*, 106–111. [CrossRef]
41. Huang, Y.; Talreja, R. Statistical analysis of oblique crack evolution in composite laminates. *Compos. B Eng.* **2014**, *65*, 34–39. [CrossRef]
42. Xia, Z.P.; Yu, J.Y.; Cheng, L.D.; Liu, L.F.; Wang, W.M. Study on the breaking strength of jute fibres using modified Weibull distribution. *Compos. Part A Appl. Sci. Manuf.* **2009**, *40*, 54–59. [CrossRef]
43. Sia, C.V.; Nakai, Y.; Shiozawa, D.; Ohtani, H. Statistical analysis of the tensile strength of treated oil palm fiber by utilisation of Weibull distribution model. *Open J. Compos. Mater.* **2014**, *4*, 72–77. [CrossRef]
44. Saba, N.; Paridah, M.T.; Abdan, K.; Ibrahim, N.A. Fabrication of epoxy nanocomposites from oil palm nano filler: Mechanical and morphological properties. *BioResources* **2016**, *11*, 7721–7736. [CrossRef]
45. Balaji, A.; Karthikeyan, B.; Raj, C.S. Morphological and mechanical behavior of sugarcane bagasse fibers reinforced polyester eco-friendly biocomposites. *J. Chem. Pharm. Res.* **2015**, *7*, 573–577.
46. Arrakhiz, F.Z.; Malha, M.; Bouhfid, R.; Benmoussa, K.; Qaiss, A. Tensile, flexural and torsional properties of chemically treated alfa, coir, and bagasse reinforced polypropylene. *Compos. B Eng.* **2013**, *47*, 35–41. [CrossRef]
47. Cerqueira, E.F.; Baptista, C.A.R.P.; Mulinari, D.R. Mechanical behavior of polypropylene reinforced sugarcane bagasse fibers composites. *Procedia Eng.* **2011**, *10*, 2046–2051. [CrossRef]
48. Vilay, V.; Mariatti, M.; Taib, R.M.; Todo, M. Effect of fiber surface treatment and fiber loading on the properties of bagasse fiber-reinforced unsaturated polyester composites. *Compos. Sci. Technol.* **2008**, *68*, 631–638. [CrossRef]

49. Marques, M.F.; Melo, R.P.; Araujo, R.S.; Lunz, J.N.; Aguiar, V.O. Improvement of mechanical properties of natural fiber–polypropylene composites using successive alkaline treatments. *J. Appl. Polym. Sci.* **2015**, *12*, 132. [CrossRef]
50. Inacio, W.P.; Lopes, F.P.D.; Monterio, S.N. Diameter dependence of tensile strength by Weibull analysis: Part III sisal fiber. *Rev. Mater.* **2010**, *15*, 124–130. [CrossRef]
51. Bevitori, A.B.; Da Silva, I.L.A.; Lopes, F.P.D.; Monterio, S.N. Diameter dependence of tensile strength by Weibull analysis: Part II jute fiber. *Rev. Mater.* **2010**, *15*, 117–123. [CrossRef]
52. Monterio, S.N.; Lopes, L.P.D.; Ferreira, A.S.; Nascimento, D.C.O. Natural fiber polymer matrix composites: Cheaper, tougher and environmentally friendly. *JOM* **2009**, *61*, 17–22. [CrossRef]
53. Siti Alwani, M.; Abdul Khalil, H.P.S.; Islam, M.N.; Sulaiman, O.; Zaidon, A.; Dungani, R. Microstructural Study, Tensile Properties, and Scanning Electron Microscopy Fractography Failure Analysis of Various Agricultural Residue Fibers. *J. Nat. Fibers* **2015**, *12*, 154–168. [CrossRef]
54. Defoirdt, N.; Biswas, S.; Vriese, L.; Tran, L.Q.N.; Acker, J.V.; Ahsan, Q.; Gorbatikh, L.; Vuure, A.V.; Verpoesta, I. Assessment of the tensile properties of coir, bamboo and jute fiber. *Compos. Part A Appl. Sci. Manuf.* **2010**, *41*, 588–595. [CrossRef]
55. Sawpan, M.A.; Pickering, K.L.; Fernyhough, A. Effect of various chemical treatments on the fibre structure and tensile properties of industrial hemp fibres. *Compos. A Appl. Sci. Manuf.* **2011**, *42*, 888–895. [CrossRef]
56. de Farias, J.G.; Cavalcante, R.C.; Canabarro, B.R.; Viana, H.M.; Scholz, S.; Simão, R.A. Surface lignin removal on coir fibers by plasma treatment for improved adhesion in thermoplastic starch composites. *Carbohydr. Polym.* **2017**, *165*, 429–436. [CrossRef] [PubMed]
57. Faludi, G.; Dora, G.; Imre, B.; Renner, K.; Móczó, J.; Pukánszky, B. PLA/lignocellulosic fiber composites: Particle characteristics, interfacial adhesion, and failure mechanism. *J. Appl. Polym. Sci.* **2014**, *131*, 39902. [CrossRef]
58. Renner, K.; Kenyo, C.; Móczó, J.; Pukánszky, B. Micromechanical deformation processes in PP/wood composites: Particle characteristics, adhesion, mechanisms. *Compos. A Appl. Sci. Manuf.* **2010**, *41*, 1653–1661. [CrossRef]

Disclaimer/Publisher's Note: The statements, opinions and data contained in all publications are solely those of the individual author(s) and contributor(s) and not of MDPI and/or the editor(s). MDPI and/or the editor(s) disclaim responsibility for any injury to people or property resulting from any ideas, methods, instructions or products referred to in the content.